Predictions in Ungauged Basins: Promise and Progress (Proceedings of symposium S7 held during the Seventh IAHS Scientific Assembly at Foz do Iguaçu, Brazil, April 2005). IAHS Publ. 303, 2006.

Investigation of the effect of a coupled land–atmosphere satellite data assimilation system on land–atmosphere processes

SOUHAIL BOUSSETTA, TOSHIO KOIKE, MAHADEVAN PATHMATHEVAN & KUN YANG

Dept of Civil Engineering, University of Tokyo, 7-3-1, Hongo, Bunkyo-ku, Tokyo 113-8656, Japan

souhail6@hydra.t.u-tokyo.ac.jp

Abstract The objective of this study is to develop a new downscaling approach, which can take into account atmospheric and land surface heterogeneities for a better precipitation prediction. We address the effect of land surface heterogeneity on the land–atmosphere interactions through coupling a land data assimilation system with a land–atmosphere coupled model. This system relies on a mesoscale model as the atmospheric part, a Land Surface Scheme as a model operator, a Radiative Transfer Model as an observation operator, satellite data and the Simulated Annealing method for minimization. To assess the effectiveness of the new system, two-dimensional numerical experiments were carried out in a mesoscale area of the Tibetan Plateau for dry and wet seasons. The results showed significant differences compared with standard regional atmospheric model outputs and were more consistent with satellite microwave brightness temperature observations. The latter induced an improvement of the spatial distribution of soil moisture, which strongly affected the convection systems.

Key words data assimilation; land surface scheme; regional model; remote sensing

INTRODUCTION

Since GCMs are still unable to produce mesoscale and local atmospheric phenomena, downscaling methods are necessary to bridge the gap between a GCM's scale, and other smaller modelling scales. One standard method is nesting using regional atmospheric models, but this approach is till now unable to reproduce local phenomena and extreme events (Xu, 1999), because nesting does not include effects of both land surface and atmospheric heterogeneities. In fact, soil moisture, as a surface boundary condition, plays important roles in the partition and estimation of surface fluxes, which in return drive the surface–atmosphere interaction. Thus it is essential that regional models include accurate and robust initial surface condition in order to capture regional atmospheric structure.

On the other hand, heterogeneity of atmospheric parameters especially precipitation, is also very important in atmospheric modelling considering its role in atmospheric thermal control through heat release and absorption.

On the way to overcome these problems, related to both land surface (soil moisture) and atmosphere (precipitation), microwave remote sensing due to its global and frequent availability is an appropriate tool for retrieving the spatial and temporal coverage of those parameters. But due to the small penetration depth of these satellite

measurements, in the case of soil moisture, they can not be directly used by regional models. Integrating satellite observation within a land surface scheme through a data assimilation process would provide soil moisture profiles physically consistent with regional model use. So, to overcome the limitations related to the standard nesting method, a new downscaling approach by the assimilation of satellite brightness temperature within a coupled land–atmosphere variational scheme would be considered to take into account both atmospheric and land surface heterogeneities.

As a first step, in this paper; we investigate the effect of introducing land surface heterogeneities on land–atmosphere interactions and their mechanisms by coupling a land data assimilation system to retrieve the whole soil moisture profile as an initial surface condition with a coupled land–atmosphere model.

A COUPLED LAND–ATMOSPHERE DATA ASSIMILATION SYSTEM

General scheme

In this study, a land data assimilation system is coupled with a coupled land–atmosphere model. This is done by first coupling a land surface scheme with a regional model to guarantee land–atmosphere interactions, then introducing the surface heterogeneity by assimilating the microwave remote sensing data into the land surface scheme and feeding back to the land–atmosphere coupled model (Fig. 1). The scheme components are explained in the following section.

The land–atmosphere coupled model

The atmospheric module As a mesoscale prediction model which includes: a land surface scheme that can reproduce surface fluxes exchanges, and a cloud microphysics

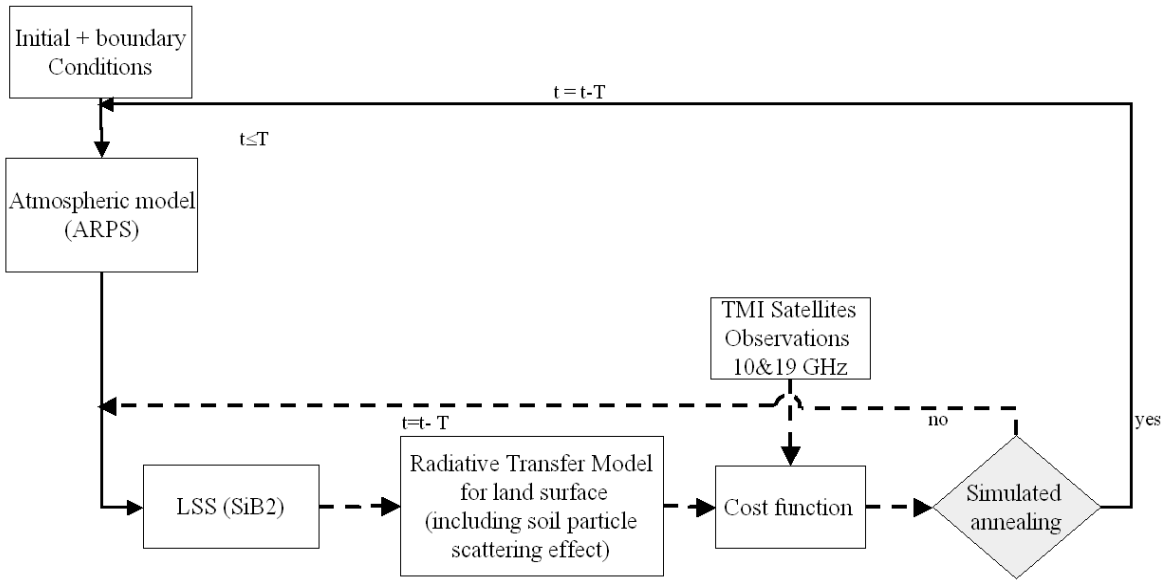

Fig. 1 Satellite data assimilation of a land atmosphere coupled system.

module that describe precipitation development, the Advanced Regional Prediction System ARPS elaborated by the Center for Analysis and Prediction of Storms at the University of Oklahoma was chosen for this study. It includes four packages: an atmospheric module, a land surface scheme, a radiation package and parameterization of cloud microphysics.

The atmospheric model is three-dimensional (3-D) and nonhydrostatic, which describes the dynamics of air motion, especially detecting the generation of convection systems. The model is governed by momentum equations, thermodynamic equation, continuity equation, three/six transport equations of water-categories, and sub-grid-scale turbulent kinetic energy (TKE) sub model. These equations are transformed from the physical domain to computational domain by the terrain-following coordinate and grid-stretching in vertical. The cloud microphysics includes the NEM (Schultz, 1995) scheme, the Kessler two-category liquid water scheme and the three-category ice scheme; also modified a Kuo cumulus convection scheme is included as well as the Kain-Fritsch convective parameterization. The radiation package includes two options for solar radiation and long-wave atmospheric radiation estimation, a simple calculation option and, a radiative transfer parameterization one. More details about ARPS are found in Xue *et al*. (1995).

The land surface scheme The land surface scheme originally included in ARPS is the ISBA (Interaction between Soil, Biosphere, and Atmosphere) developed by Noilhan & Planton (1989). Considering the improvement of soil moisture and fluxes estimation, the revised Simple Biosphere Model 2: SiB2 (Sellers *et al*., 1996) was chosen as an alternative to the ISBA. In fact the SiB2 is a dual-source model in which fluxes are originating from the soil surface and vegetation canopy. It incorporates simple representations of vertical soil moisture transport, plant-controlled transpiration, interception, evaporation, infiltration, and sensible and ground heat fluxes through physically-based mechanisms. SiB2 includes three soil layers: a surface soil layer of a few centimetres, which acts as a significant source of direct evaporation when moist; a root zone, which is the supplier of soil moisture to the roots and accounts for transpiration; and a deep soil layer, which acts as a source for hydrological base flow and upward recharge of the root zone. Moreover SiB2 can handle satellite data to specify time-varying phenological properties (LAI, FPAR).

The Land Data Assimilation System

Cost function The Land Data Assimilation System (LDAS) assimilates passive microwave radiometer observations of brightness temperature into the land surface scheme. The SiB2 is used as a model operator driven by the outputs of the coupled land–atmosphere model.

The Radiative Transfer Model (RTM), as an observation operator, calculates the brightness temerature which is then compared with the satellite observation through the following cost function:

$$J(x_0)=\frac{1}{2}\sum_{i=0}^{n}(H_i[M(x_0)]-y_i^o)^T R_i^{-1}(H_i[M(x_0)]-y_i^o)+\frac{1}{2}(x_0-x_0^b)^T B^{-1}(x_0-x_0^b) \quad (1)$$

here x and M are the model's state vector (soil moistures at three different layers, surface temperature and canopy temperature) and its corresponding dynamics operator, respectively. y_i^0 is the radiometer observation at time t_i and H is an observation operator. Both H and M are nonlinear operators. R is the observational error covariance matrix and consists of instrumental and representativeness errors. B is an *a priori* weighting matrix, meant to approximate the error covariance matrix of background. Minimizing J obtains the optimal solution of above cost function (Pathmathevan *et al*., 2003).

The estimation of the error covariance matrices B and R is achieved by assuming unbiased Gaussian error distributions. The practical way to estimate the related error statistics is to assume that they are stationary over a period of time and uniform over a domain so they can be empirically estimated through a number of error realizations since errors cannot be observed directly. In this study, the specification of the matrix B was done using statistics on the departure between many 24 h and 48 h forecasts, while for matrix R the measurement errors added to the brightness temperature values were assumed to have a standard deviation of 1K.

Radiative transfer model Based on the emission behaviour of dry soil and liquid water in the microwave region, a physically-based radiative transfer model was developed by Koike *et al*. (2000), allowing the estimation of soil moisture from the land surface expressed as follows:

$$\begin{aligned} T_{BT} &= T_{bs} \exp(-\tau_c) \exp(-\tau_r) \\ &+ [(1-\varpi_c)(1-\exp(-\tau_c))\, T_c] \exp(-\tau_r) \\ &+ \sum_{i=1}^{N} (1-\varpi_{r_i})(\exp(-\tau_{r_i}))\, T_{r_i} \end{aligned} \tag{2a}$$

This equation represents the total emission and attenuation from the land surface (s), vegetation canopy (c), and rainfall drop (r). Continuously, T_{BT} is the brightness temperature at the measurement level, T_{bs} is the brightness temperature at the ground level, T is the actual temperature, τ is the optical depth, ω is the single scattering albedo, and N is the total number of rain drops. Given that the atmosphere and rain are transparent at lower frequencies, the third term of the right hand side of the above equation is neglected (Fuji *et al*., 2000).

τ_C is the vegetation optical depth function of the vegetation water content w_e computed after Jackson *et al*. (1991):

$$\tau_C = b w_e / \cos\theta \tag{2b}$$

where b is a coefficient that depends on the canopy structure and frequency.

The dielectric constant of the soil that is mainly dependent on our assimilation variable (soil moisture) is computed after Dobson *et al*. (1985).

In order to consider the soil particle scattering effect in dry soil, the 4 Stream Fast Radiative Transfer Model, originally developed for the atmosphere (Liu, 1998), was used to compute the outcoming brightness temperature at the ground level T_{bs}, which is then included in equation (2a).

Assuming the soil medium as a parallel plane azimuthally symmetric containing spherical soil particles, the radiative transfer process to derive T_{bs} can be expressed by:

$$\mu \frac{d}{d\tau}\begin{bmatrix} I_v(\tau,\mu) \\ I_h(\tau,\mu) \end{bmatrix} = \begin{bmatrix} I_v(\tau,\mu) \\ I_h(\tau,\mu) \end{bmatrix} - (1-\omega_0)B_p(\tau)\begin{bmatrix} 1 \\ 1 \end{bmatrix} - \frac{\omega_0}{2}\int_{-1}^{1}\begin{bmatrix} P_{VV} & P_{VH} \\ P_{HV} & P_{HH} \end{bmatrix}\begin{bmatrix} I_v(\tau,\mu') \\ I_h(\tau,\mu') \end{bmatrix} d\mu' \quad (2c)$$

where, $I_v(\tau,\mu)$,[$I_h(\tau,\mu)$] is the radiance at optical depth ($\tau = \kappa_e dz$) in direction μ for vertical or [horizontal] polarization, ω_0 is the single scattering albedo of soil particle, $B_p(\tau)$ is the Plank function and $P_{ij}(i, j = H \text{ or } V)$ is the scattering phase function.

Liu had efficiently solved this model (equation (2c)), by expressing the scattering phase function with the Henyey-Greenstein formula (1941), assuming a non cross polarization, limiting the number of streams to four and using the discrete ordinate method.

Simulated annealing A heuristic optimization approach called Simulated Annealing (SA), which is capable of minimizing the cost function without using adjoint models is used in this system. SA allows avoiding problems due to strong nonlinearity and discontinuity, in finding the global minimum in the hilly structure of the cost function. It is based on an analogous approach to the metal annealing in thermodynamics (William *et al*., 1992).

Coupled assimilation cycle In order to have a continuous scheme (Courtier, 1997), the coupled assimilation cycle is performed as follows: first, the coupled land–atmosphere model (ARPS-SiB2) is run for an assimilation window time T to give an initial guess and forcing parameters for the Land Data Assimilation System (LDAS); and second, the LDAS is run for one assimilation window which then feedbacks the new surface initial condition for the coupled model at time $t = t - T$; third, the coupled model is run for two assimilation windows 2T, the first window output is then considered as the optimal one and the second will serve as forcing for the next LDAS run.

NUMERICAL EXPERIMENT

The Tibetan Plateau was chosen for this study, firstly because it has a heterogeneous soil moisture distribution resulting from its mountain-valley topographical structure, and an active convection system (Yang *et al*., 2004), and secondly because of its available comprehensive data sets collected during the GAME IOP 1998 project.

To investigate the effect of the coupled system on the different land surface and atmospheric outputs and mechanism, a 2-D numerical experiment was preferred to a 3-D one for its computational efficiency and its ability to effectively address the physical mechanisms rather than focusing on any observational validation.

On the other hand, knowing that the westerly is dominating the flow in the Tibetan Plateau, which implies that the west–east direction have more homogeneous atmospheric and surface conditions than the north–south direction (Yang *et al*., 2004), a 250-km section running south to north and centred at (31.750°N, 91.635°E) was selected as our experimental domain.

To be able to trace the land surface heterogeneities and to detect the generation of convective systems, a 5 km spatial resolution was considered.

In order to assess the system efficiency on a wide range of climate conditions, the experiments were performed during a Monsoon period (July) as a wet season, then during a pre-Monsoon period (May) as a dry season.

The lateral boundary conditions were set to periodic in order to avoid external and bigger scale atmospheric effect on our domain. And, for a fast and complete parametrization of the cloud, the NEM microphysics scheme was applied with an explicit convective resolution.

For the LSS (SiB2), the three soil layers were set to 0–4 cm, 4–20 cm and up to 150 cm for the deep layer. The vegetation type in the Tibetan plateau corresponds to grassland which is C4 class in SiB2 according to Sellers *et al*. (1996). Other static parameters associated with land cover and soil were obtained from Sellers *et al*. (1996) and the Game-Tibet experiment.

The radiative transfer model parameters were also estimated according to the Game-Tibet experiment (Koike *et al*., 1999), and the TMI (TRMM Microwave Imager) brightness temperature of 10.65 and 19.35 GHz were used in the assimilation scheme.

RESULTS AND DISCUSSION

The coupled land–atmosphere assimilation system was tested during a wet period (5–10 July 1998) and a dry period 20–25 May 1998), by two numerical experiments each: a coupled land–atmosphere model ARPS-SiB2 case run without assimilation referred as (noAss) and an assimilation case where ARPS-SiB2 is coupled in a continuous cycle with land data assimilation, referred in the following sections as (Ass).

Wet season

Being a very complex variable in atmospheric modelling due to its integration of the surface local state, as well as both local and synoptic atmospheric state, precipitation is the most difficult variable to predict. In this experiment, the precipitation results (Fig. 2) showed that although both cases started from the same wet atmospheric conditions, the noAss case generated much less precipitation than the assimilation Ass case because the soil condition was wetter due to its correction by the observed estimates through the land data assimilation scheme. In fact Fig. 3 shows that in the noAss case soil moisture, gradually dry up from 20% to less than 5%, while in the Ass cases it shows an increase of the soil moisture to higher values. This is mainly due to the reason that observed satellite data processed through the radiative transfer model gave higher and more realistic values to the coupled model. The higher amount of precipitation in the Ass case is also explained by the higher values of latent heat flux, and lower values of sensible heat flux (Fig. 4) being consistent to the actual flux partition in Tibet during the Monsoon season (Fig. 5). An increase of soil moisture tends to increase the latent heat flux and therefore atmospheric moisture, while at the same time it decreases the sensible heat flux and therefore the air temperature. These changes work in the same direction to increase relative humidity making precipitation more intense and frequent. This suggests that the precipitation generation in the Tibetan Plateau is strongly influenced by the soil moisture conditions.

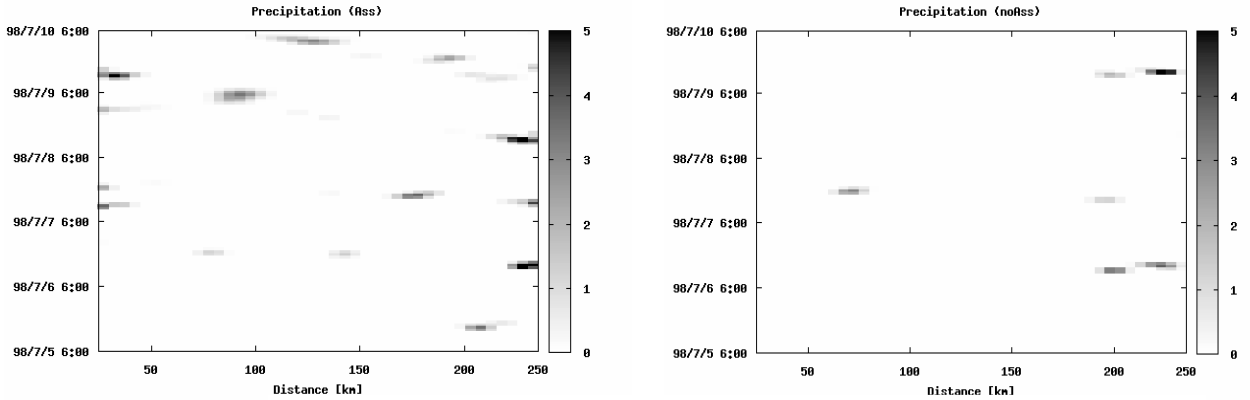

Fig. 2 Temporal/spatial distribution of precipitation (wet season).

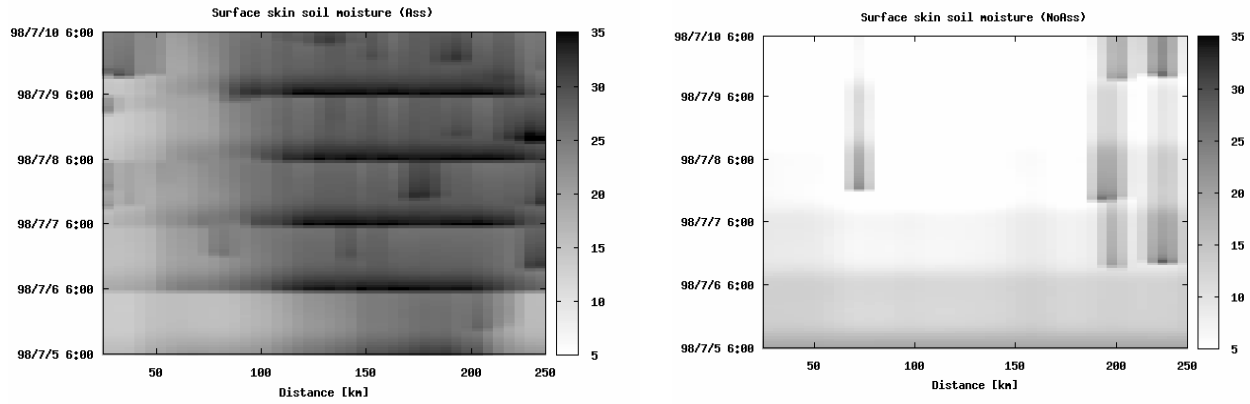

Fig. 3 Temporal/Spatial surface soil moisture distribution (wet season).

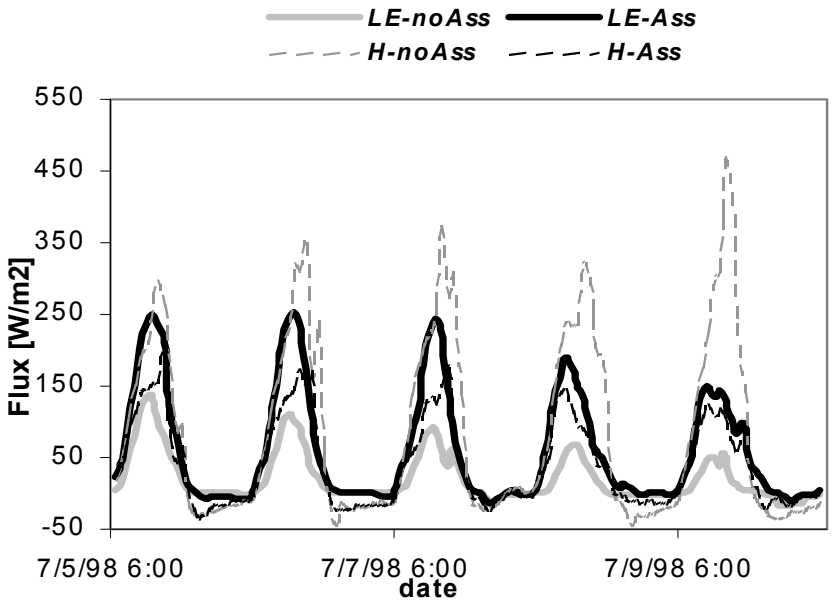

Fig. 4 Spatially averaged fluxes (wet season).

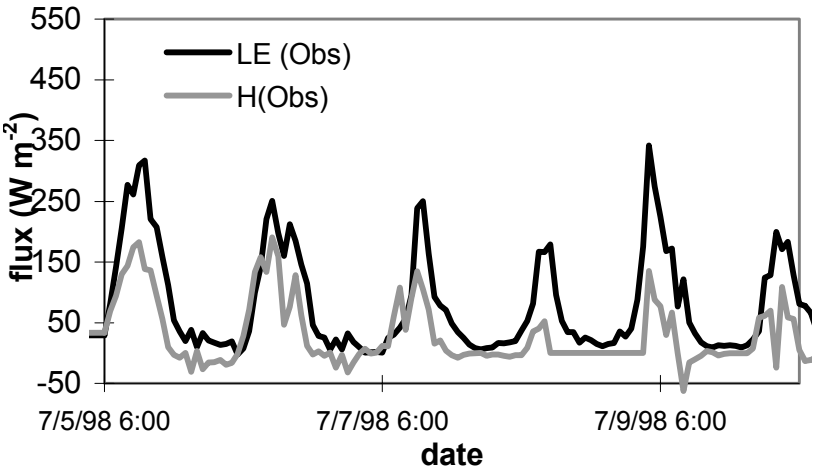

Fig. 5 Observed surface fluxes at Amdo station (wet season).

To confirm this hypothesis, the local convection systems as drivers of precipitation were also investigated. During the day, the sun heats the ground and evaporates water into the air, subsequently the air near the surface become unstable allowing air parcels from the surface layer to rise and thus initiating the convection process. A useful measure of this process is the Lifted Index which expresses the difference of the rising parcel equivalent potential temperature with its surrounding environment. In Fig. 6, we plotted the spatio-temporal distribution of the lifted index for the Ass and noAss cases. In the Ass case, more atmospheric instability was observed (Li < –4) due to wet convection, which resulted in more frequent precipitation events than in the NoAss case. In fact in this case, vertical motion initiated the deep convection and thus enhanced the vertical moisture transport.

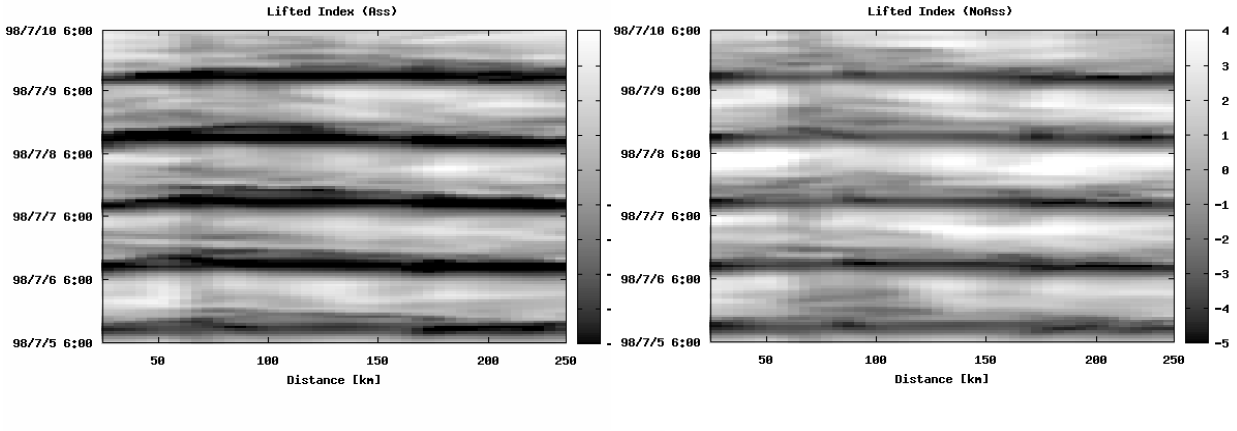

Fig. 6 Temporal/spatial lifted index distribution (wet season)

Dry season

In the dry season case, the precipitation (Fig. 7) also showed different spatial and temporal pattern for the assimilation and non-assimilation cases. This can be also

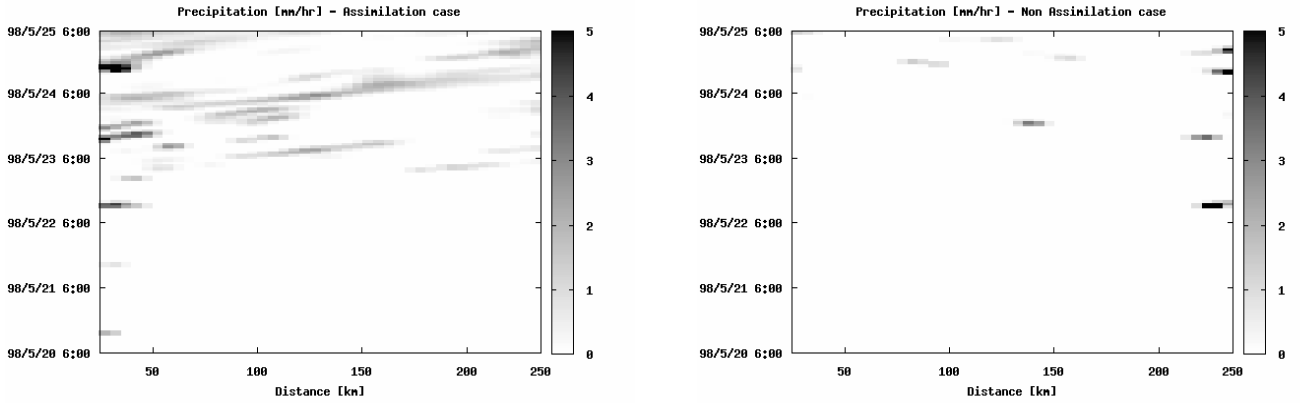

Fig. 7 Temporal/spatial precipitation distribution (dry season).

explained by the different soil moisture conditions and their related interaction with the atmosphere.

Figure 8 shows that in the no assimilation case, a clear diurnal cycle was observed ranging from 13% during noon time to approximately 17% in the early morning, mostly spatially homogeneous distributed, while in the assimilation case, the updating process based on satellite observations at the beginning of each assimilation window (06:00 h local time), tended to smooth back the diurnal variation by lowering its magnitude through lowering the early morning soil moisture to drier values. Moreover, in the assimilation case, a much more heterogeneous spatial distribution was fed back to the system instead of the homogeneous one.

These soil moisture conditions influenced the surface fluxes to lead to different atmospheric stability conditions; in fact, atmospheric instability was observed in both the assimilation and non-assimilation cases, especially around noon time when solar heating is at its maximum (Fig. 9).

Moreover, the investigation of the lifting condensation level (Fig. 10) showed that the planetary boundary layer was shallower in the assimilation case, inferring the generation of the moist convection process and resulting in more frequent precipitation, especially in the last 2 days.

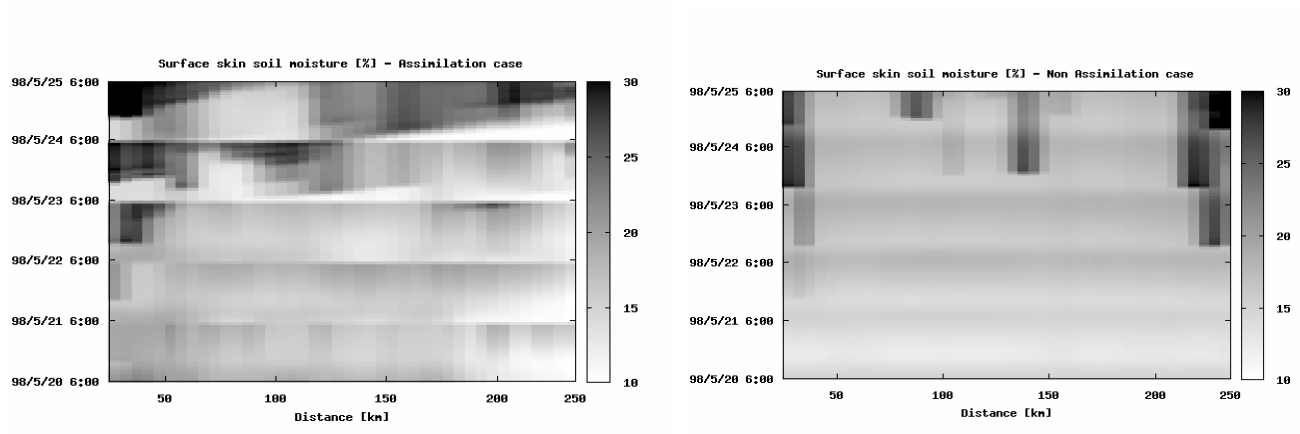

Fig. 8 Temporal/spatial surface soil moisture distribution(dry season).

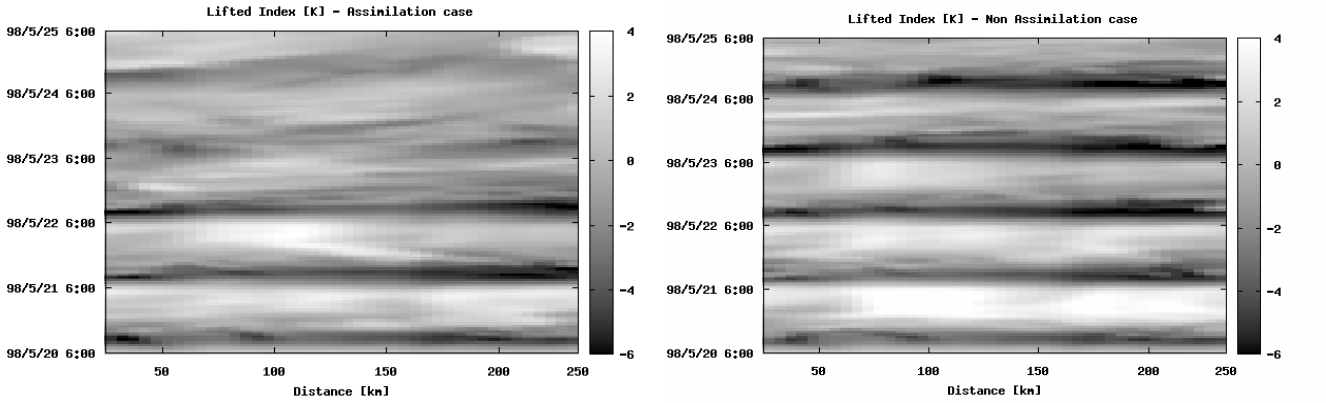

Fig. 9 Temporal/Spatial Lifted index distribution(dry season).

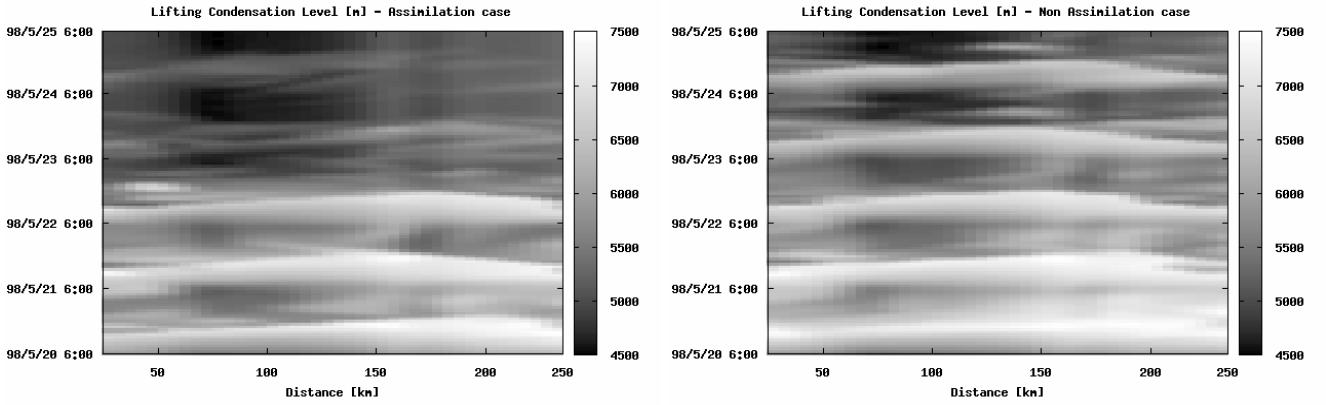

Fig. 10 Temporal/Spatial Lifting Condensation Level distribution (dry season).

In this dry season simulation, it is important to mention that even though the atmosphere was more unstable, especially in the non-assimilation case (Li < –4), precipitation did not occur as much as in the last two days of the assimilation case. This can be explained by the lack of atmospheric moisture needed to generate precipitation. Of particular importance also, the soil moisture heterogeneous pattern that encouraged the generation of small convergence zone resulting in specific vertical motion, which enhanced the moist convection process and thus precipitation (see the fourth day in Figs 7 and 8).

By coupling a land data assimilation with a coupled land–atmosphere system in a continuous way, the soil moisture became more consistent with observed satellite brightness temperature. And through the consideration of the surface heterogeneities given by the satellite observation, the assimilation system provided better spatial distribution of soil moisture, which had a strong influence on the mechanism of local convection and consequently precipitation predictability.

Acknowledgments This study was carried out as a part of Coordinated Enhanced Observing Period (CEOP) project funded by the Japan Science and Technology Agency and the Special Coordination Funds for Promoting Science and Technology. The authors would like to express their so deep gratitude to them.

REFERENCES

Courtier, P. (1997) Variational methods. *J. Met. Soc. Japan* **75**(1B): 211–218.

Dobson, M. C., Ulaby, F. T., Hallikainen, M. T. & El-Rayes, M. A. (1985) Microwave dielectric behavior of wet soil – Part II: Dielectric-mixing models. *IEEE Trans. Geosci. Rem. Sens* **GE-23**, 35–46.

Fujii, H. & Koike, T. (2000) Development of a TRMM/TMI algorithm for precipitation in the Tibetan plateau by considering effects of land surface emissivity. *J. Met. Soc. Japan* **79**, 475–483.

Henyey, L. C. & Greenstein J. L (1941) Diffuse radiation in the galaxy. *Astrophysical J.* **93**, 70–83.

Jackson, T. J. & Schmugge, T. J. (1991) Vegetation effects on the microwave emission of soils *Remote Sens. Environ*. **36**, 203–213.

Koike, T., Shimo, C. Ohta, T. Fujii, H. & Shibata, A. (2000) Development and validation of a microwave radiometer algorithm for land surface hydrology. *Ann. J. Hydraulic Engng*, JSCE **44**, 247–252.

Koike, T., Yasunari, T. Wang, J. & Yao, T. (1999) GAME-Tibet IOP summary report, In: *Proc. First Int. Workshop on GAME-Tibet* (ed. by A. Numaguti, L. Liu & L. Tian), Xi'an China, 11–13, January 1999. Chinese Academy of Sciences and Japan National Committee for GAME.

Liu, G. (1998) A fast and accurate model for microwave radiance calculations. *J. Met. Soc. Japan* **76**(2), 335–343.

Noilhan, J, & Planton, S (1989) A simple parametrization of land surface processes for meteorological models. *Mon. Weath. Rev.* **117**, 536–549.

Pathmathevan, M., Koike, T., Li, X. & Fujii, H. (2003) A simplified land data assimilation scheme and its application to soil moisture experiments in 2002 (SMEX02). *Water Resour. Res.* **39**(12), 1341.

Press, W. H., Flannery, B. P., Teukolsky, S. A. & Vetterling, W. T. (1992) *Numerical Receipes in C: The Art of Scientific Computing*. Cambridge University Press, Cambridge, UK.

Schultz, P. (1995) An explicit cloud physics parameterization for operational numerical weather prediction. *Mon. Weath. Rev.* **123**, 3331–3343.

Sellers, P. J., Los, S. O., Tucker, C. J., Justice, C. O., Dazlich, D. A., Collatz, G. J. & Randall, D. A. (1996) A revised land surface parameterization (SiB2) for atmospheric GCMs, Part II: the generation of global fields of terrestrial biophysical parameters from satellite data. *J. Climate* **9**, 706–737.

Ulaby, F. T., Moore, R. K. & Fung, A. K. (1982) *Microwave Remote Sensing Active and Passive* (Vol. 2). *Microwave Remote Sensing Fundamentals and Radiometry*. Artech House, London, UK.

Xu, C. (1999) From GCMs to river flow: a review of downscaling methods and hydrologic modelling approaches. *Progr. Phys. Geogr.* **23**(2), 229–249.

Xue, M. Droegemeier, K. K. Wong, V. (1995): The Advanced Regional Prediction System (ARPS)—A multi-scale nonhydrostatic atmospheric simulation and prediction model. Part I: Model dynamics and verification *Meteor. Atmos. Phys*. **75**, 161–193.

Yang, K., Koike, T., Fujii, H., Tamura, T., Xu, X., Bian, L. & Zhou, M. (2004) The daytime evolution of the atmospheric boundary layer and convection over the Tibetan Plateau: observations and simulations. *J. Met. Soc. Japan*. **82**(6), 1777–1792.